Int. J. Nav. Archit. Ocean Eng. (2015) 7:500~508
http://dx.doi.org/10.1515/ijnaoe-2015-0036
pISSN: 2092-6782, eISSN: 2092-6790

Hydrodynamic modeling of semi-planing hulls with air cavities

Konstantin I. Matveev

School of Mechanical and Materials Engineering Washington State University

Received 3 December 2014; Revised 22 February 2015; Accepted 17 March 2015

ABSTRACT: *High-speed heavy loaded monohull ships can benefit from application of drag-reducing air cavities under stepped hull bottoms. The subject of this paper is the steady hydrodynamic modeling of semi-planing air-cavity hulls. The current method is based on a linearized potential-flow theory for surface flows. The mathematical model description and parametric calculation results for a selected configuration with pressurized and open air cavities are presented.*

KEY WORDS: Semi-planing boat; Stepped hull; Air cavity ship; Method of hydrodynamic singularities.

INTRODUCTION

Fast, shallow-draft, high-payload monohulls are often used for landing military operations. At sufficiently high speeds, these boats move in the semi-planing mode with the hull weight supported by both hydrostatic and hydrodynamic forces. For reducing hull drag by about 10-20% and increasing boat speed, air cavity systems can be applied on the hull bottom (Fig. 1). Stable air cavities can substantially reduce frictional resistance by decreasing the wetted surface area. A review of early developments of air-cavity ships and boats is given by Latorre (1997).

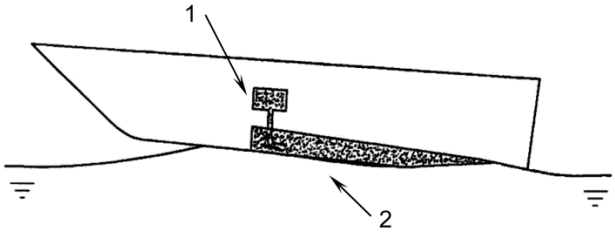

Fig. 1 Air-cavity hull schematic. 1, air blower; 2, air cavity.

Air-cavity landing craft and small fast ferries are already built in series (Matveev, 2005). However, several cases of unsuccessful developments of air-cavity boats are also known (e.g., Tudem, 2002; Dize, 2008). The problem of designing high-performance air-cavity hulls is caused by their more complex hydrodynamics and limited engineering knowledge on this subject in the public domain, including mathematical models for air-cavity flows near hulls. Some developments of numerical methods for planing and displacement hulls are described by Butuzov (1988), Choi et al. (2005), and Thill et al. (2005).

This paper presents a potential-flow method for calculating hydrodynamics of semi-planing hulls with air cavities. The current approach originates from previous models developed by the author for modeling stepless planing hulls at finite Froude

Corresponding author: *Konstantin I. Matveev*, e-mail: *matveev@wsu.edu*

numbers, air cavities under horizontal walls, and two-dimensional air-cavity stepped hull forms (e.g., Matveev, 2007; Matveev and Ockfen, 2009; Matveev, 2012). Some physical and geometrical simplifications are employed here for the sake of computational efficiency and clarity of the concept presentation. The next section contains an outline of the mathematical model and is followed by calculation examples and discussion.

MATHEMATICAL MODEL

For modeling hydrodynamics of a semi-planing hull with an air cavity, a potential-flow method of hydrodynamic sources is employed. The problem schematic is shown in Fig. 2. The air cavity is formed behind a transverse step on the hull bottom. The air cavity is usually restricted from the sides by narrow skegs; their width is neglected in the present formulation. The water flow is assumed to be inviscid, irrotational and steady. The dynamic boundary condition on the water surface is expressed via Bernoulli equation for the water surface streamlines,

$$p_0 + \frac{1}{2}\rho U_0^2 = p + \frac{1}{2}\rho U^2 + \rho g\, y_w\,, \tag{1}$$

where p_0 and U_0 are the pressure and velocity in the far upstream undisturbed water surface at $y = 0$, ρ is the water density, and $p(x,z)$ and $U(x,z)$ are the pressure and velocity on the water surface with elevation $y_w(x,z)$. Assuming small trim angles of the hull and sufficiently high hull speeds, flow disturbances caused by the hull presence can be considered to be relatively small. Therefore, the wave slopes and the x-axis velocity perturbation $u = U_x - U_0$ will be small as well. Then, the Bernoulli equation on the free water surface can be linearized and written as follows,

$$\frac{1}{2}\sigma = \frac{u}{U_0} + 2\pi\frac{y_w}{\lambda}\,, \tag{2}$$

where $\sigma = (p_0 - p)/(\rho U_0^2/2)$ is the cavitation number (zero on the free surface open to atmosphere and non-zero on the surface of a pressurized cavity between the hulls) and $\lambda = 2\pi U_0^2/g$ is the wavelength on the unconstrained free water surface. The air cavity pressure is treated here as an input parameter. On the wetted hull surface, the same Eq. (2) holds as well, but an unknown and space-dependent pressure coefficient with minus sign is used instead of the cavitation number, i.e., $C_p = (p - p_0)/(\rho U_0^2/2) = -\sigma$.

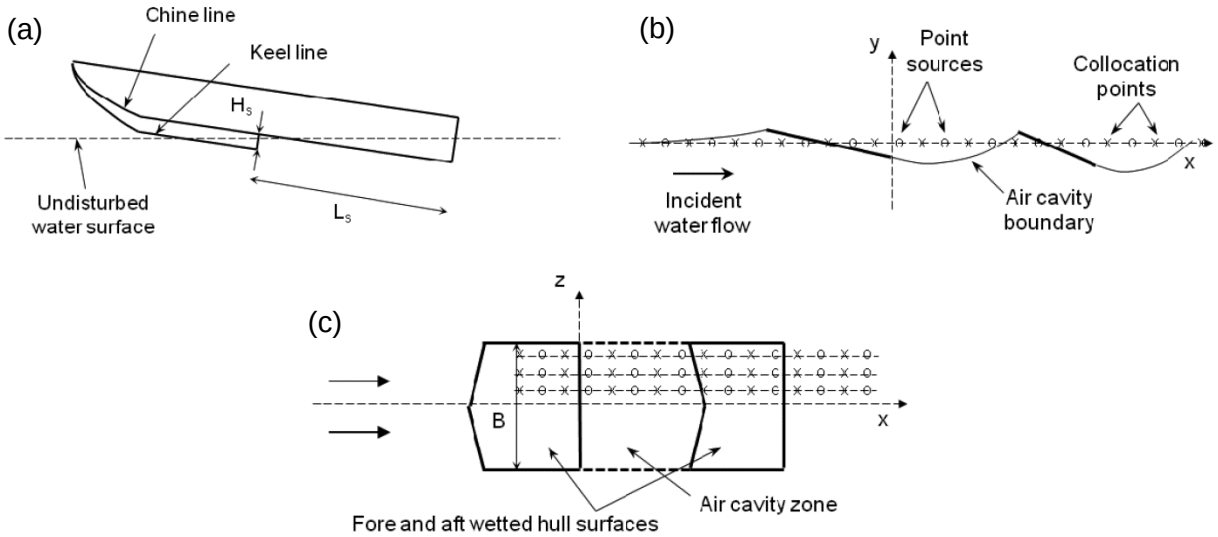

Fig. 2 (a) Side view of a stepped hull. (b) longitudinal cross-section. (c) top view. Circles, point sources; crosses, collocation points. Only a small part of the numerical domain and a small fraction of sources and collocation points are shown.

The water flow disturbances induced by the hull are modeled with hydrodynamic sources distributed over a horizontal plane at $y = 0$ (Fig. 2). A velocity potential of each source satisfies the Laplace equation in the fluid domain. The collocation points, where Eq. (2) is fulfilled, are shifted upstream from the sources. This staggered arrangement minimizes the influence of the downstream boundary of the numerical domain (Bertram, 2000). Then, the x-component of the velocity perturbation is determined from the source intensities as follows,

$$u(x_i, z_i) = \frac{1}{4\pi} \sum_j \frac{q_j}{r_{i,j}^2} \frac{x_i - x_j^s}{r_{i,j}}, \tag{3}$$

where (x_i, z_i) and (x_j^s, z_j^s) are the coordinates of the collocation point i and the source j with intensity q_j, and $r_{i,j} = \sqrt{(x_i - x_j^s)^2 + (z_i - z_j^s)^2}$ is the horizontal distance between these points. The linearized kinematic boundary condition on the water surface results in the additional relation between the source intensities and the water surface slope (Matveev 2013),

$$\frac{1}{2\Delta z}\left(\frac{q_{i-1}}{\Delta x_{i-1}} + \frac{q_i}{\Delta x_i}\right) = -2U_0 \frac{\partial y_w}{\partial x}(x_i, z_i), \tag{4}$$

where q_{i-1} and q_i are the source strengths of the upstream and downstream neighbors of the collocation point i, and Δx and Δz are the intervals between the source locations in x and z directions. On the hull surface, the slope is known; therefore, the source intensities can be directly related to the local trim angle of the hull. The linear system of equations (Eqs. (2)-(4)) is solved for the water surface elevations outside the hull, pressure coefficients on the hull, source intensities, and velocity perturbations. The lift force on the hull and the center of pressure are then determined from pressure distribution on the hull surface and the cavity area.

One complication in the considered problem is the initially unknown wetted sections of the hull, since the water tends to rise ahead of the planing surface (Fig. 1). In order to determine the water rise, an iterative solution procedure is applied. Initially, the front points of the wetted surfaces are selected as intersections of the undisturbed water plane and the hull bottom line. After finding a solution, a water rise in front of the hull is calculated and more accurate estimate for the wetted length is obtained. The calculations are repeated until the elevation of the water at the impinging point becomes equal to the hull vertical coordinate at this location. In addition, the water spray that can appear above the water rise line is neglected similar to Riabouchinsky model commonly used in developed cavitating flows (Knapp et al., 1970).

The conducted mesh-converging studies in the range of conditions used in this work suggested the following recommendations for dimensions of numerical cells and the entire domain. The distances between sources on the hull and cavity in both x- and z-directions are should be selected at most as $B/8$, where B is the hull beam. Outside of the hull, Δx gradually increases towards the front and back boundaries of the numerical domain (to make computations faster), but it is capped by the value $\lambda/20$. The distances in front and on the sides of the hull up to the domain boundaries are chosen as $1.5B$; and the distance from the hull transom to the downstream domain boundary is taken as $6B$. Selecting finer cells or larger domain does not significantly change calculated hydrodynamic characteristics of the hull.

RESULTS

The validation of any numerical method is a necessary step toward its practical application. Unfortunately, test data with complete description of experimental conditions and results for semi-planing air-cavity hulls are not available in the open technical literature. Instead, a comparison of results of the current method is made here with two experiments of related configurations.

The first test data set for air-cavity lengths was obtained with a simplified model-scale air-cavity hull tested in a recirculating water channel (Matveev et al., 2009). In the experiments, the hull length, beam and height were 55.8 *cm*, 30.5 *cm* and 9.8 *cm*, respectively. The hull was nearly two-dimensional, except for 0.95-*cm*-high, 0.64-*cm*-wide skegs on two sides of the cavity section. In front of the step, there was 2.5-*cm*-long flat plate, and the bow section was made in a parabolic shape approaching zero slope at the flat section. The hull was tested in a fixed position at two submergences H (Fig. 3(a)), 1.3 *cm* and 4.1 *cm*, and

zero trim, whereas the water flow velocities U_0 were in the range 28-86 *cm/s*. One of the main measured variables was the air cavity length L (Fig. 3(a)). The test data in the normalized form are shown by symbols in Fig. 3(b), whereas curves correspond to modeling results. Froude number in the figure is defined as $Fr_H = U_0 / \sqrt{gH}$. The agreement between experimental and numerical results is very good in the range of studied conditions.

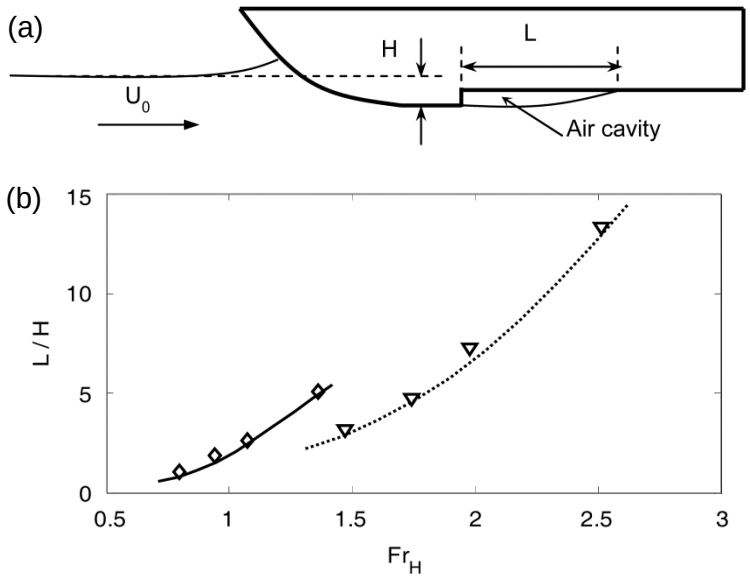

Fig. 3 (a) Schematic of tested hull model. (b) cavity length. Diamonds and solid curve, deep submergence. Triangles and dotted curve, shallow submergence. Fr_H is Froude number based on the step submergence.

The second validation comparison is made here for a stepless planing hull operating at relatively low Froude numbers, including the semi-planing regime (Begovic and Bertorello, 2012). This hull had a long bottom section with fixed deadrise angle β = 16.7° and a curved bow piece with unspecified geometry. In computations by the current method, all wetted hull portion was treated as having a constant deadrise. In the experiments, the hull was free to move; trim angles varied between 1.8° and 4.2°, whereas a relative change of the vertical position of the center of gravity $y_{cg} / V^{1/3}$ (with V being the hull displacement) was between -0.05 and 0.09. The authors provided all test information in a table format (Begovic and Bertorello, 2012), and these data were used in the present calculations. The experimental and modeled lift coefficient, $C_L = F / (0.5\rho U_0^2 B^2)$, with F being the lift force, and the mean wetted length are shown in Fig. 4. The agreement between modeling and experimental data is satisfactory, accounting for the fact that the actual wetted surface included a small part of the curved bow piece.

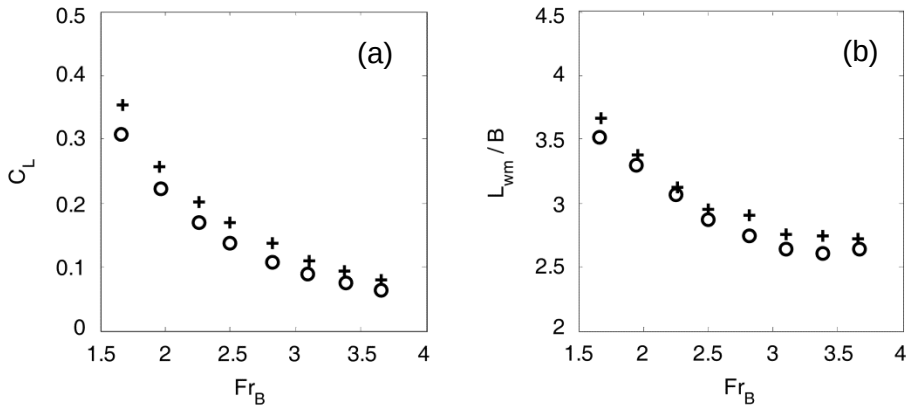

Fig. 4 (a) Lift coefficient and (b) mean wetted length of a planing hull. Crosses, current method; circles, test data (Begovic and Bertorello, 2012).

The presented comparisons can be treated as a partial validation of the current numerical method for air-cavity hulls. However, more results of well-described experiments with such hulls are needed in order to carry out complete validation. It should be mentioned that the present method has been previously validated for several other related configurations, including near-hull/hydrofoil wake wash (Matveev and Ockfen, 2009) and a cavity behind a supercavitating wedge (Matveev and Miller, 2011).

Upon the partial validation of the present numerical approach, parametric calculations have been conducted in this study for one selected configuration of a semi-planing hull form. The boat relative volumetric displacement is chosen as $V/B^3 = 0.8$ (where V is the dimensional displacement and B is the hull beam), whereas the center of gravity is positioned from the hull transom at the relative distance $L_{cg}/B = 2.8$. The forebody deadrise is 5° (constant within its wetted area), while the aftbody deadrise is chosen to be zero as often implemented on real air-cavity hulls. The aftbody base plane is parallel to the forebody keel line. The distance between the step and the hull transom is $L_s = 3B$. The step height (H_s in Fig. 2(a)) and the beam Froude number, $Fr_B = U_0/\sqrt{gB}$, are the variable input parameters.

Two values for pressure inside the air cavity formed behind the step are considered in this study. From experience with air-cavity hulls (e.g., Matveev et al., 2009), the cavity pressure is often found to be slightly less than the hydrostatic pressure at the step level. Since the forebody has a finite deadrise angle, the cavity gage pressure is realistically estimated here as the hydrostatic pressure at the chine submergence level h_c (in the step cross-section), i.e., $p_c = \rho g h_c$. In the second case, the cavity gage pressure is taken as zero. This corresponds to a conventional stepped planing hull with a cavity that directly communicates with the atmosphere.

The output parameters in calculations include the step submergence at the keel line h_1 and the hull trim angle τ. These values correspond to equilibrium conditions, when the total lift (including force due to cavity pressure) is equal to the selected boat weight and the center of pressure acts through the given center of gravity. The equilibrium states are not known in advance. They are found iteratively by varying the hull submergence and trim until the sum of vertical forces and their moments become zero.

Another output parameter of primary practical interest is the hull drag D. It is estimated here as a sum of the lift-induced and friction components of resistance, D_L and D_F. The lift-induced (pressure) drag is essentially the lift force L multiplied by a small hull trim angle τ. A minor force acting on the area A_s on the back side of the step due to elevated pressure in the cavity is subtracted to get more accurate estimate,

$$D_L = L\tau - p_c A_s . \tag{5}$$

The friction resistance is simply evaluated through the combined wetted area of the hull A_w,

$$D_F = C_f \frac{\rho U_0^2}{2} A_w , \tag{6}$$

where C_f is the effective friction coefficient selected here to be equal to a realistic value of 0.004. It should be noted that other resistance components, such whisker spray drag and appendage drag, are neglected for simplicity.

The first set of parametric calculations is carried out for a variable step height H_s and a fixed Froude number, $Fr_B = 2$. This calculation can be considered as a part of a search for the optimal hull geometry at the given boat speed. Non-dimensional results for the drag, attitude parameters (sinkage and trim), and minimum value of the wetted length on the aftbody L_2 are shown in Fig. 5 for hulls with pressurized and open cavities. The weight of the hull relates to the volumetric displacement as $W = \rho g V$. In the case of the air-cavity hull (with $p_c > 0$), drag monotonically decreases with increasing step height (Fig. 5(a)), which is caused primarily by reduction of the wetted area on the aftbody (correlated with L_2 in Fig. 5(b)) despite some increase of the submergence (Fig. 5(c)) and trim (Fig. 5(d)). However, in practice it is desirable to keep a certain amount of wetted area on the aftbody to avoid flow instabilities and sudden loss of the pressurized cavity that can happen when it reaches the atmosphere at the hull transom; this may occur in unsteady hull motions in waves, maneuvers, etc. In the present study, a safe value for the minimum wetted length on the aftbody is chosen as $B/3$, which is shown by a dotted line in Fig. 5(b). Therefore, the most optimal step height in the considered set is $H_s = 0.1B$.

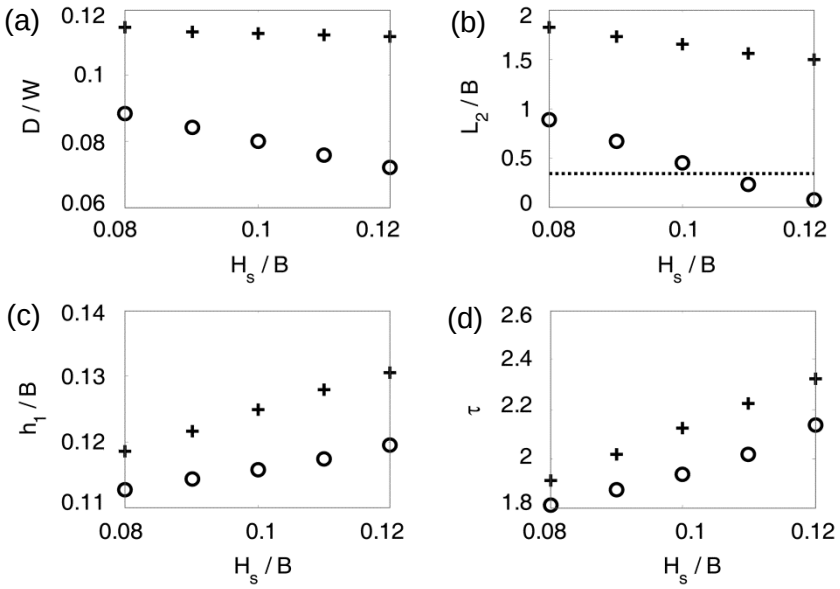

Fig. 5 (a) Drag-to-weight ratio, (b) normalized minimum wetted length on aftbody, (c) normalized step submergence, (d) trim angle (in degrees). Circles, air-cavity hull with pressurized cavity; crosses, stepped planing hull with open cavity. Dotted line in (b) depicts the selected threshold for minimum wetted length.

Results for the stepped planing hull with an open cavity are shown in Fig. 5 by crosses. Its drag is substantially higher than that of the air-cavity hull (Fig. 5(a)) due to larger wetted area and higher trim angle (Fig. 5(d)), since the open air cavity does not produce any lift. The drag of this hull is found to be less sensitive to the variation of the step height in the selected conditions (Fig. 5(a)). The decrease of the aftbody wetted area (correlated with L_2 in Fig. 4(b)) is nearly compensated by more pronounced increases in the step submergence and trim (Fig. 5(c), (d)).

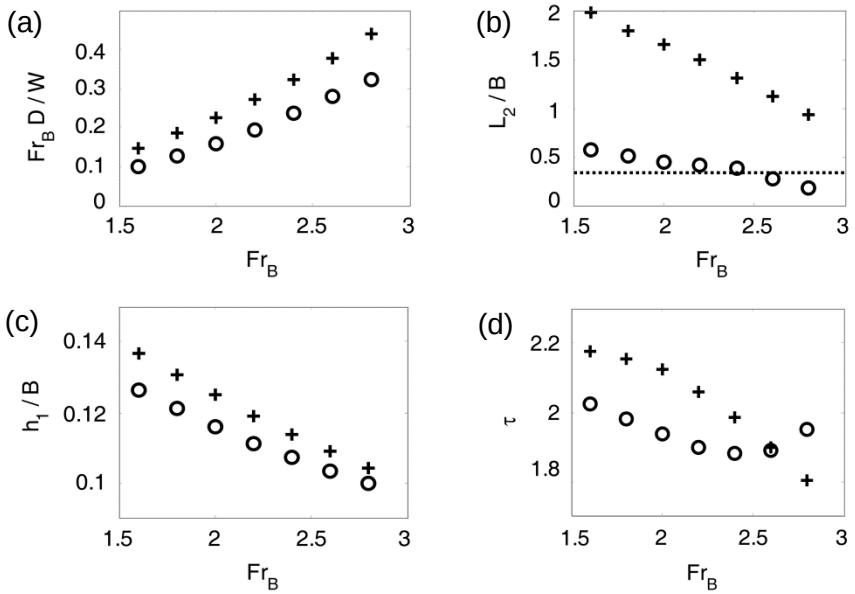

Fig. 6 (a) Normalized propulsive power, (b) normalized minimum wetted length on aftbody, (c) normalized step submergence, (d) trim angle (in degrees). Circles, air-cavity hull; crosses, stepped planing hull. Dotted line in (b) depicts the threshold for minimum wetted length.

The second calculation set is obtained for the hull with $H_s / B = 0.1$, same loading (mass and center of gravity) and other geometrical parameters, and variable Froude number (or boat speed). Results are presented in Fig. 6 for the non-dimensional combination proportional to the required propulsive power $P = DU_0 \sim Fr_B D / W$, the minimal wetted length of the aftbody

L_2, and the hull sinkage and trim. Again, the air-cavity hull with a pressurized cavity is more efficient in the studied range than the stepped planing hull with an open cavity (Fig. 6(a)). The required power monotonically increases with increasing Froude number. The wetted length L_2 decreases with Fr_B; and it becomes smaller than the selected here critical value of $B/3$ at $Fr_B = 2.6$. Hence, this air-cavity hull can robustly operate at speeds up to $Fr_B = 2.4$. The sinkage of both hulls, as well as the trim of the open-cavity setup, decreases with Fr_B due to higher hydrodynamic lift per submerged area (Fig. 6(c)). In the air-cavity setup, the trim starts increasing at high Froude numbers due to drastic reduction of lift-producing wetted area on the aftbody (Fig. 6(d)).

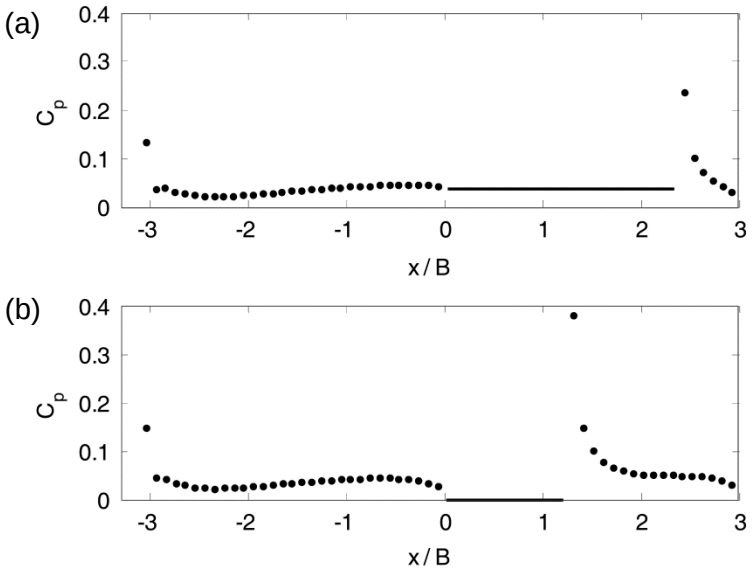

Fig. 7 Pressure coefficient distribution at ¼-buttock line. Points, on the hull surface; solid line, inside the air cavity. (a) air-cavity hull, (b) stepped planing hull.

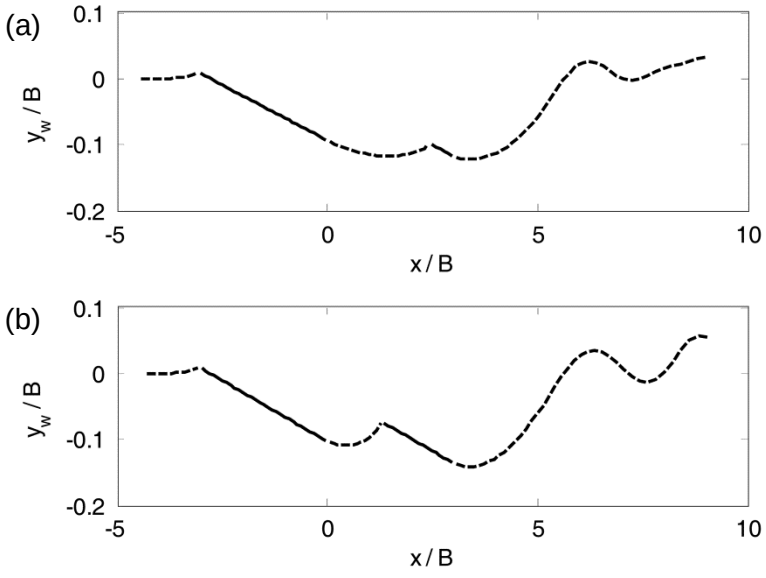

Fig. 8 Water surface elevation at ¼-buttock line. (a) air-cavity hull, (b) stepped planing hull.

Examples of pressure coefficient distributions and water surface elevations at ¼-buttock lines on the air-cavity hull with a pressurized cavity and the stepped planing hull with an open cavity are shown in Figs. 7 and 8. In this condition, the step height is $H_s = 0.1B$ and Froude number is $Fr_B = 2$. One can notice the longer cavity with higher pressure on the air-cavity hull, whereas the stepped planing hull has higher trim, longer wetted lengths, and a cavity with zero gage pressure. The pressure

distributions on fore and aft bodies resemble those of a single planing hull (Fig. 7). The pressure is maximum at the leading points of the wetted lengths. There is a local maximum (albeit relatively small) closer to the trailing point on the forebody, which is caused by stronger hydrostatic contribution on deeper submerged portions of the hull. The pressure on the aftbody is generally higher since they operate in the upwash flow caused by the forebody.

The water surface elevations around these hulls are illustrated in Fig. 9. Some features in the wave patterns are similar to other fast hulls: there are wave hollows behind transoms followed by a focused water elevation ("rooster tail") and divergent water waves. The hull bottom area covered with the air cavity is substantially larger in the pressurized setup. The front water lines on the aftbodies are quite different. In the case of the open cavity (Fig. 9(b)), it resembles a parabolic shape of the wave hollow formed by the forebody. In the case of the pressurized cavity (Fig. 9(a)), this shape is inverted, so that the maximum wetted length is at the hull centerline, whereas minimum wetted length are at the sides. This pattern is typically observed on real air-cavity hulls that have low-deadrise aft sections (Matveev, 1999).

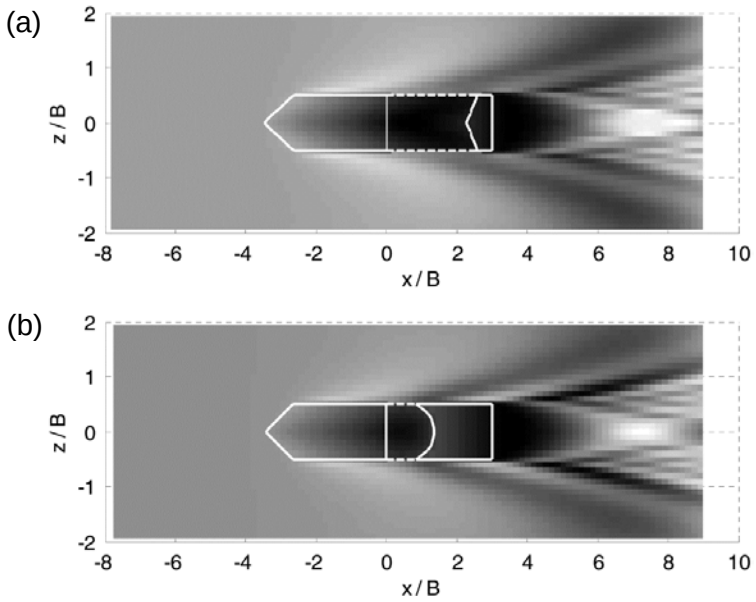

Fig. 9 Water surface contours around (a) air-cavity hull and (b) stepped planing hull of the same loading and speed. Brightness is proportional to the water surface elevations. Solid white lines surround wetted hull areas. Dashed white lines indicate lateral boundaries of the air cavity.

CONCLUSIONS

The water flow around simplified hull forms of a semi-planing boat with an air cavity has been modeled with a computationally efficient potential-flow method. Partial validation was conducted, but more experimental data are needed to achieve more confidence in the current approach that shows a promise for the practical boat design. Parametric calculations are presented for a stepped hull with pressurized and open cavities, illustrating the influence of the step height and Froude number. The present method is also capable of modeling wave patterns and determining shapes of hull wetted surfaces, which suggests a possibility of further studies of the hull features on the air-cavity boat performance, including aftbody deadrise, wetted skegs with finite width, multi-cavity setups, and propulsors.

ACKNOWLEDGEMENT

This material is based upon work supported by the National Science Foundation under Grant No. CMMI-1026264.

REFERENCES

Begovic, E. and Bertorello, C., 2012. Resistance assessment of warped hullform. *Ocean Engineering*, 56, pp.28-42.

Bertram, V., 2000. *Practical ship hydrodynamics*. Oxford: Butterworth-Heinemann.

Butuzov, A.A., 1988. Spatial linearized problems on flow around ship with artificial cavitation. *Shipbuilding Problems, Ship Design Series*, 8, pp.1-18.

Choi, J.-K., Hsiao, C.-T. and Chahine, G.L., 2005. Design trade-off analysis for high performance ship hull with air plenums. *Proceedings of the 2nd International Symposium on Seawater Drag Reduction*, Busan, Korea, 23-26 May 2005, pp.1-16.

Dize, A.P., 2008. Quadrapod air-assisted catamaran hull. *Proceedings of the 1st Chesapeake Power Boat Symposium*, Annapolis, MD, 7-8 March 2008, pp.1-6.

Knapp, R.T., Daily, J.W. and Hammit, F.G., 1970. *Cavitation*. New York: McGraw-Hill.

Latorre, R., 1997. Ship hull drag reduction using bottom air injection. *Ocean Engineering*, 24(2), pp.161-175.

Matveev, K.I., 1999. Modeling of vertical plane motion of an air cavity ship. *Proceedings of the 5th International Conference on Fast Sea Transportation*, Seattle, WA, 31 August - 2 September 1999, pp.463-470.

Matveev, K.I., 2005. Application of artificial cavitation for reducing ship drag. *Oceanic Engineering International*, 9(1), pp.35-41.

Matveev, K.I., 2007. Three-dimensional wave patterns in long air cavities on a horizontal plane. *Ocean Engineering*, 34 (13), pp.1882-1891.

Matveev, K.I., Burnett, T. and Ockfen, A., 2009. Study of air-ventilated cavity under model hull on water surface. *Ocean Engineering*, 36(12-13), pp.930-940.

Matveev, K.I. and Ockfen, A., 2009. Modeling of hard-chine hulls in transitional and early planing regimes by hydrodynamic point sources. *International Shipbuilding Progress*, 56(1-2), pp.1-13.

Matveev, K.I., and Miller, M.J., 2011. Air cavity with variable length under model hull. *Journal of Engineering for the Maritime Environment*, 225(2), pp.161-169.

Matveev, K.I., 2012. Two-dimensional modeling of stepped planing hulls with open and pressurized air cavities. *International Journal of Naval Architecture and Ocean Engineering*, 4, pp.162-171.

Matveev, K.I., 2013. Hydrodynamics of tandem planing surfaces. *Proceedings of the SNAME Annual Meeting*, Bellevue, WA, 6-8 November 2013, pp.1-7.

Thill, C., Toxopeus, S. and van Walree, F., 2005. Project energy-saving air-lubricated ships (PELS). *Proceedings of the 2nd International Symposium on Seawater Drag Reduction*, Busan, Korea, 23-26 May 2005, pp.1-16.

Tudem, U.S., 2002. The challenge of introducing innovative Air Lifted Vessels to the commercial market. *Proceedings of the 18th Fast Ferry Conference*, Nice, France, 26-28 February 2002, pp.1-10.